Evidence for Iron Channeling in the Fet3p−Ftr1p High-Affinity Iron Uptake Complex in the Yeast Plasma Membrane†

Ernest Y. Kwok, Scott Severance, and Daniel J. Kosman*

Department of Biochemistry, School of Medicine and Biomedical Sciences, State University of New York at Buffalo, Buffalo, New York 14214

Received October 24, 2005; Revised Manuscript Received March 28, 2006

ABSTRACT: In high-affinity iron uptake in the yeast *Saccharomyces cerevisiae*, Fe^{II} is oxidized to Fe^{III} by the multicopper oxidase, Fet3p, and the Fe^{III} produced is transported into the cell via the iron permease, Ftr1p. These two proteins are likely part of a heterodimeric or higher order complex in the yeast plasma membrane. We provide kinetic evidence that the Fet3p-produced Fe^{III} is trafficked to Ftr1p for permeation by a classic metabolite channeling mechanism. We examine the ^{59}Fe uptake kinetics for a number of complexes containing mutant forms of both Fet3p and Ftr1p and demonstrate that a residue in one protein interacts with one in the other protein along the iron trafficking pathway as would be expected in a channeling process. We show that, as a result of some of these mutations, iron trafficking becomes sensitive to an added Fe^{III} chelator that inhibits uptake in a strictly competitive manner. This inhibition is not strongly dependent on the chelator strength, however, suggesting that Fe^{III} dissociation from the iron uptake complex, if it occurs, is kinetically slow relative to iron permeation. Metabolite channeling is a common feature of multifunctional enzymes. We constructed the analogous ferroxidase, permease chimera and demonstrate that it supports iron uptake with a kinetic pattern consistent with a channeling mechanism. By analogy to the Fe^{III} trafficking that leads to the mineralization of the ferritin core, we propose that ferric iron channeling is a conserved feature of iron homeostasis in aerobic organisms.

In iron uptake by most organisms, reduction of environmental Fe^{III} to Fe^{II} by metalloreductases serves to labilize the more insoluble, exchange-inert ferric ion. This reductive mobilization makes the iron more bioavailable to an organism's extracellular or plasma membrane iron trafficking components, e.g., a siderophore or a divalent metal ion transporter like DMT1/Nramp2 (*1*−*3*). Reoxidation then converts the more labile Fe^{II} to the ferric ion that can be stably transported (siderophore, transferrin) or stored (ferritin). This reoxidation must be tightly coupled to metalloreduction since Fe^{II} is a prooxidant that has the potential to produce the one-electron reduction products of dioxygen, the superoxide and hydroxyl radicals, and the two-electron reduction product, hydrogen peroxide, that itself is a prime source of the cytotoxic hydroxyl radical (*4*, *5*). The oxidase step in this iron metabolic process must be tightly coupled to the iron handling component, also; if it is not, the Fe^{III} produced will likely be lost to hydrolysis, thereby setting up a futile cycle of reductive solubilization followed by an autoxidation leading to re-formation of insoluble ferric hydroxide(s).

The redox nature of iron metabolism is well illustrated by the mechanism of high-affinity iron uptake in the yeast *Saccharomyces cerevisiae*. *S. cerevisiae* produces several metalloreductases (*6*−*8*). The Fre1 protein contributes 90−95% of plasma membrane reductase activity while Fre2p contributes the remainder (*9*). The high-affinity uptake of this reductase-generated Fe^{II} is due to the Fet3 and Ftr1 proteins (*10*, *11*). Biochemical and genetic data suggest that Fet3p and Ftr1p form a complex in the yeast plasma membrane that could be a heterodimer or higher order oligomer (*11*−*13*). Fet3p is a multicopper oxidase (*14*, *15*) and, like ceruloplasmin (*16*) and hephaestin (*17*), two multicopper oxidases required for mammalian iron metabolism, exhibits specificity toward Fe^{II} as substrate, thus catalyzing what is known as the ferroxidase reaction (*2*, *15*, *18*). Ftr1p functions as the iron permease in this high-affinity iron uptake pathway (*11*, *13*).

Fet3p is a type 1 membrane protein with a single transmembrane domain. The topology and orientation of Fet3p is amino-terminal out and carboxyl-terminal in; the multicopper oxidase (MCO)[1] motifs are within the 555 amino acid residue amino-terminal, exocellular domain (*18*, *19*) (Figure 1). As a multicopper oxidase, Fet3p possesses the three distinct types of copper sites that have been characterized in copper proteins (*14*, *15*, *19*−*22*). Thus, Fet3p has one type 1, or blue copper site; one type 2, or nonblue copper site; and one binuclear copper cluster, designated a type 3 site, in which the unpaired electrons on the two cupric ions in the cluster are spin-coupled. The T2 and T3 copper atoms form a trinuclear cluster. Oxidation (ferroxidation) of Fe^{II}

† This research was supported by National Institutes of Health Grant DK53820.

* Correspondence should be addressed to this author. Phone: 716-829-2842. Fax: 716-829-2661. E-mail: camkos@buffalo.edu.

[1] Abbreviations: MCO, multicopper oxidase; G(Y/C)FP, green (yellow/cyan) fluorescent protein; UTR, untranslated region; MES, 2-(*N*-morpholino)ethanesulfonic acid; PM, plasma membrane; NTA, nitrilotriacetate; HEDTA, hydroxyethylenediaminetriacetic acid; ORF, open reading frame.

10.1021/bi052173c CCC: $33.50
Published on Web 04/26/2006

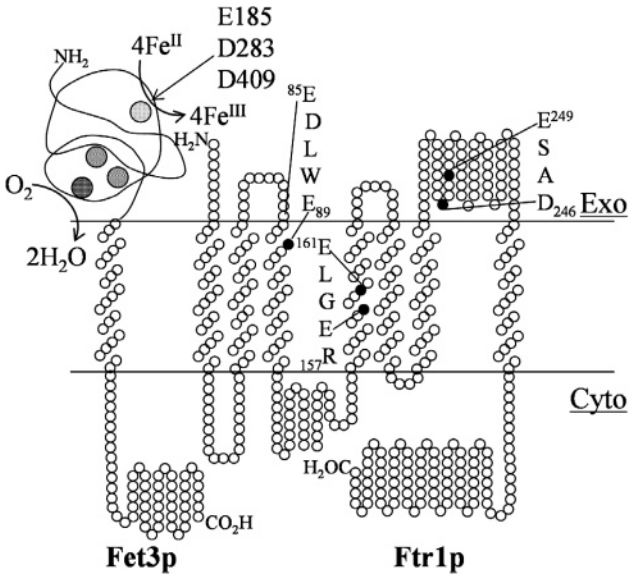

FIGURE 1: Structural models of Fet3p and Ftr1p in the yeast plasma membrane. Fet3p has a single transmembrane domain, and Ftr1p has seven; the proteins share an N_{exo}/C_{cyt} topology (*13*). Fet3p residues E185, D283, and D409 at this enzyme's type 1 copper ferroxidase site contribute to Fe trafficking from Fet3p to Ftr1p (*28*) as do Ftr1p residues E89, D246, and E249. Ftr1p contains REXLE motifs in transmembrane domains 1 and 4; the R and E residues in each motif are essential to Fe permeation (*13*).

occurs at the type 1 copper site, while dioxygen is reduced to $2H_2O$ at the trinuclear cluster (*14*, *22*).

Ftr1p has seven transmembrane domains and an amino-terminal exocytoplasmic, carboxyl-terminal cytoplasmic (N_{exo}/C_{cyt}) orientation (*13*). A cartoon depicting this model is included in Figure 1, which also indicates two REXLE motifs found in two of the predicted transmembrane domains and a ^{246}DASE^{249} motif in exocellular loop 6. Each of the four glutamic acid residues in the former two motifs is required for iron uptake through Ftr1p while the D246 and E249 residues in the loop 6 motif together make a significant contribution to iron permeation (*13*). Ftr1p residue E89 at the interface of the plasma membrane and exocellular space also is required for full Fe uptake activity (*13*). These data indicate that each of these motifs is part of the Fe permeation process that chaperones the Fe^{III} produced by Fet3p in the exocytoplasmic space into the cytoplasm (*11*, *13*).

The fact most fundamental to the elucidation of the mechanism of iron uptake through the Fet3p−Ftr1p complex is that uptake per se is absolutely *coupled* to ferroxidation (*3*, *10*, *15*). As much as iron binding to transferrin or iron accumulation in ferritin requires the oxidation of ferrous to ferric iron, iron permeation through Ftr1p *requires* that ferroxidation catalyzed by Fet3p is ongoing. While Fre1p/Fre2p can be by-passed by presenting the yeast cell with exogenous Fe^{II}, Fet3p cannot be by-passed by presenting the cell with exogenous Fe^{III}. This coupling suggests a model in which the Fe^{III} product of the Fet3p ferroxidase reaction is channeled to Ftr1p for subsequent uptake. This model, in turn, suggests that there are residues in both proteins associated with this trafficking process, e.g., the glutamic and aspartic acid residues in Ftr1p noted above.

The objective of the current study was to obtain evidence in support of this channeling model for the trafficking of Fe^{III} in the Fet3p−Ftr1p complex. Specifically, we provide kinetic data for iron uptake that fit to a thermodynamic model for a functional interaction between residues on the two proteins in support of iron permeation. Kinetic evidence is shown also that Fe^{III} produced by Fet3p can be trapped by Fe^{III} chelators but that this inhibition of uptake is conditioned by the presence of mutations in exocytoplasmic residues in Fet3p and in Ftr1p required for iron trafficking in the complex. We show that the effectiveness of a chelator in inhibiting iron uptake in this way does not correlate strongly to its Fe^{III} chelator strength, indicating that chelating agents are possibly accessing Fe^{III} bound to the permease complex and not scavenging Fe^{III} released to bulk solvent. Last, a Fet3p, Ftr1p chimera is described for which these kinetic tests demonstrate that an artificial, bifunctional ferroxidase: permease fusion exhibits the features common to metabolite channeling in other bifunctional proteins.

MATERIALS AND METHODS

Strains, Media, and Culture Conditions. The strain used in these studies was AJS05, which was derived from DEY1457 (*MAT*α can1 his3 leu2 trp1 ura3 ade6) (*23*). The AJS05 genotype is *MAT*α can1 his3 leu2 trp1 ura3 ade6 fet3::HIS3 ftr1::TRP1 aft1::AFT1-1^{up}KAN. The *AFT1-1*^{up} allele codes for a constitutively active form of the Aft1p transcription factor that drives expression of the *FET3* (and *FTR1*) locus (*24*). In this background, expression of episomally expressed wild-type and mutant alleles of *FET3* and *FTR1* and of the chimeric genes was maximized, affording cultures that contained the protein partners in the plasma membrane as described. Overnight cultures were grown in selective media (6.67 g/L yeast nitrogen base without amino acids, 2% glucose plus the appropriate drop-out mixture of amino acids). Early log phase cells ($OD_{660\ nm} = 0.8-2.0$) were used for all experiments.

Plasmid Construction. The plasmids containing the wild-type and mutant *FTR1* coding sequences were based on plasmid p703FTR1; this plasmid and the construction of these mutants have been described (*13*). The plasmids containing the wild-type and mutant *FET3* coding sequences were based on plasmid pDY133 and have been described (*25*). Both plasmids are maintained at low copy in yeast, and each contains the same *FET3* promoter element to ensure relatively equivalent expression. Plasmids for expressing Fet3pMCO:Ftr1p-GFP chimeras were constructed in the plasmid pJBS04-01. pJBS04-01 contains the complete *FTR1* transcription unit modified by the addition of a yEGFP coding sequence fused in-frame to the 3′ end of *FTR1* (*13*). Both chimera 1:GFP (C1:GFP) and chimera 2:GFP (C2:GFP) were produced by subcloning a fragment of the *FET3* promoter and ORF that encodes Fet3pMCO residues 1−555 into the 5′ terminus of pJBS04-01. This Fet3pMCO coding sequence was derived from the plasmid pDY148 which encodes a truncated form of Fet3p (amino acid residues 1−555) that is secreted from yeast cells but maintains ferroxidase activity (*19*). Fet3pMCO fragments including the 5′UTR were inserted in-frame into pJBS04-01 such that a single open reading frame encoding Fet3pMCO:FTR1p:GFP was created under the control of the *FET3* promoter. In the case of C1:GFP, an 11 amino acid linker region (including a FLAG epitope) joins Fet3pMCO residue G555 to residue M1 of Ftr1p. In the case of C2:GFP, a 29 amino acid linker region (including a FLAG epitope, 6×His, and thrombin

cleavage site) was used to connect the Fet3pMCO and Ftr1p-encoding DNA sequences. Subcloning was performed by Quickchange mutagenesis (Stratagene, La Jolla, CA) and standard molecular biology techniques. All DNA products were confirmed by automated fluorescent sequencing on an ABI PRISM 377 instrument.

Fluorescent Imaging of Yeast Cells (13). Images of live cell (GFP and YFP fusion) fluorescence were obtained by confocal fluorescence microscopy using a Bio-Rad MRC 1024 confocal system equipped with a 15 mW krypton/argon laser and operating on a Nikon Optiphot upright microscope and an oil immersion 60 × 1.4 NA objective. Optical sections were acquired at 0.5 μm, and the XY resolution was set at $\geq$0.2 μm using Bio-Rad's Lasersharp V3.0 software and later processed using Confocal Assistant V4.02.

Fluorescence Quantification of Fet3 and Ftr1 Fusion Proteins (13). Cells producing wild-type and mutant forms of Fet3:CFP and Ftr1:YFP were grown as above and then washed twice with 25 mM Tris, pH 6.8; cells were assayed at 6×10^6 cells/mL of the same buffer. Fluorescent protein production in these cells was determined by scanning fluorescence emission spectroscopy using a Perkin-Elmer Model LS50B luminescence spectrometer. The FL-Win Lab software, Firmware E5, was used to collect the emission spectra and then to correct these spectral envelopes for the autofluorescence of cells expressing nonfluorescent protein controls. The resulting difference spectral envelopes, which were the signal-averaged values from four scans, were quantified to yield the relative abundance of the several fluorophore-tagged protein species. As shown in Supplementary Information (Figure S1) only one sample differed from wild type by more than 20%.

Iron Uptake Assay. Iron uptake assays were performed as described (*13*, *25*). Briefly, cells were washed and resuspended in uptake buffer [0.1 M MES, pH 6.0, containing 2% (w/v) glucose and Fe^{III} chelator as indicated]. Cells (10^7/mL of uptake buffer) were added to uptake buffer containing 20 mM ascorbate and incubated with shaking for 15 min. ^{59}Fe (to the concentration indicated in the figures) was added to initiate the uptake reaction. Triplicate samples (1 mL each) were quenched in 3 mL of an ice-cold solution of 0.1 mM Tris−succinate (pH 6.0) containing 1 mM EDTA and then washed four times with this quench buffer. Samples were counted on a Wallac model 1480 Wizard γ counter with correction made for nonspecific cell accumulation of ^{59}Fe using the uptake values measured for the parental AJS05 strain (*fet3*Δ*ftr1*Δ). The uptake values given are taken from a linear uptake range, 1−10 min; for a given uptake condition triplicate samples were quantified. Curve fitting and statistical analyses of three to five sets of such data for each experiment were performed using Prism3 software (GraphPad, San Diego, CA). V_{max} and K_M values were obtained by fitting v versus [^{59}Fe] data to the Michaelis−Menten equation. Inhibition of uptake at [^{59}Fe] = 0.2 μM ($\approx K_M$) by added Fe^{III} chelator was analyzed by fitting v versus [chelator] to the equation for simple competitive inhibition (*26*):

$$v = \frac{V_{max}(\text{app})}{1 + [\text{chelator}]/K_I} \quad (1)$$

RESULTS

Iron Trafficking Residues on Fet3p and Ftr1p Interact in Iron Uptake: Kinetic Evidence for Iron Channeling. Residues in both Fet3p and Ftr1p that are required for wild-type iron trafficking and uptake by this iron permease complex have been identified by site-directed mutagenesis (*13*, *25*, *27*, *28*). For example, Fet3p(E185A) exhibits a 10-fold increase in the K_M for Fe^{II} in ferroxidation, showing that this residue contributes to iron binding to Fet3p (*25*). This contribution has been demonstrated directly by magnetic circular dichroism measurements with wild-type and mutant Fet3p species in the presence of Fe^{II}; Fe^{II} binding to wild-type Fet3p is clearly observed whereas no such binding to Fet3p(E185A) can be detected (*29*). Fet3p(E185A) has an even more dramatic phenotype in iron uptake; although this mutant Fet3p assembles with Ftr1p in an uptake complex in the yeast plasma membrane, this complex is inactive in ^{59}Fe accumulation (*25*). This difference suggests that E185 plays a role in Fe^{II} binding for ferroxidation and in trafficking Fe^{III} to Ftr1p for permeation as well. D283 and D409 appear to play comparable roles; all three acidic residues are part of the ferroxidase site in Fet3p as is apparent in the crystallographically determined structure of the protein (*28*). Several glutamate (and one aspartate) residues in Ftr1p are essential for iron permeation, also (*13*). These include four glutamate residues in two transmembrane domains, a glutamate residue (E89) at the exocytoplasmic space−plasma membrane interface, and a DASE motif found in exocytoplasmic loop 6. These elements were noted in the model of the Fet3p−Ftr1p complex illustrated in Figure 1.

We used mutants of these several motifs to obtain evidence consistent with a channeling mechanism of Fe trafficking in the Fet3p−Ftr1p complex in the following way. First, on the basis of a standard velocity versus [^{59}Fe] analysis, we obtained the fitted kinetic constants for iron uptake through wild-type and mutant complexes. There were three of the latter chosen for this analysis: Fet3p(E185D)−Ftr1p; Fet3p−Ftr1p(D246N/E249Q), designated also Ftr1p(NASQ); and the double mutant complex, Fet3p(E185D)−Ftr1p(NASQ). Using the values for K_M and V_{max} provided by this kinetic analysis, values for V_{max}/K_M were calculated as a standard measure of the uptake efficiency of the various complexes (*30*). These were then analyzed further in regard to whether the thermodynamic change(s) reflected by a change in this constant for the two single mutants was (were), in the double mutant, simply additive or, possibly, synergistic. As reviewed in more detail in the Discussion, a greater than additive effect is evidence for a functional if not physical interaction between the residues mutated in the Fe uptake "transition state" (V_{max} effect) (*31*−*34*).

The experimental velocity versus [^{59}Fe] values for these four uptake complexes in the yeast plasma membrane are shown in Figure 2. The lines in the figure are the nonlinear, theoretical fits of these data to the Michaelis−Menten equation using the fitted constants given in Table 1; the values for V_{max}/K_M are given there, also. These latter values show that the complexes containing a single mutation were as efficient as wild type in Fe uptake. In contrast, the double mutant exhibited an efficiency that was ~60% of the wild-type value with the caveat that this difference was marginally significant (see footnote to Table 1). This apparent synergy

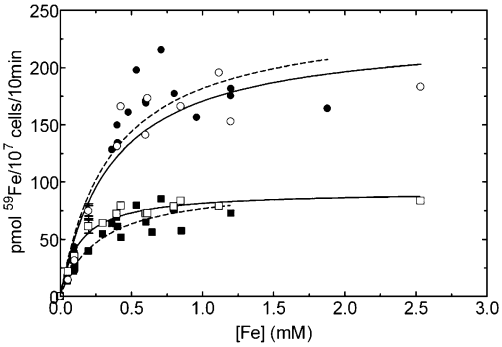

FIGURE 2: Kinetic analysis of ^{59}Fe uptake in wild-type and mutant Fet3p−Ftr1p complexes. The *fet3*Δ*ftr1*Δ-containing strain, AJS05, episomally produced combinations of wild-type or mutant forms of Fet3p and Ftr1p as indicated. ^{59}Fe uptake was programed with the [^{59}Fe] indicated in the presence of 20 mM ascorbate (reductase-independent uptake) at pH = 6.0 and 50 μM MES containing 2% glucose (w/v). ^{59}Fe accumulation was determined over 10 min (linear uptake); the values were corrected for uptake in the untransformed AJS05 control. Each data point is the mean of replicate measurements (n = 3). Each line was generated by a fit of a complete data set to the Michaelis−Menten equation; the fitted constants and their SEM are given in Table 1. The Fet3p−Ftr1p combinations used were as follows: Fet3p−Ftr1p (wild type), open circles (solid line); Fet3p(E185D)−Ftr1p, filled circles (dashed line); Fet3p−Ftr1p(D246N/E249Q), open squares (solid line); and Fet3p-(E185D)−Ftr1p(D246N/E249Q), filled squares (dashed line).

Table 1: Kinetic Constants for ^{59}Fe Uptake through Wild-Type and Mutant Fet3p−Ftr1p Complexes[a]

Fet3p−Ftr1p in complex	V_{max} (pmol of ^{59}Fe per 10^7 cells per 10 min)	K_M (μM)	V_{max}/K_M
WT-WT	231.3 ± 21.8	0.36 ± 0.09	642.5 ± 211
WT-NASQ	92.0 ± 4.1	0.13 ± 0.02	707.7 ± 140
E185D-WT	246.1 ± 23.8	0.35 ± 0.09	703.1 ± 247
E185D-NASQ	97.3 ± 7.8	0.25 ± 0.06	389.2 ± 125[b]

[a] Strain AJS-05 (*fet3*Δ*ftr1*Δ*AFT1-1*^{UP}) was cotransformed with low-copy empty vectors (negative control) or vectors containing either wild-type (WT-WT, positive control) or mutant alleles of *FET3* and *FTR1* as indicated. Fe uptake in these transformants was determined as a function of [^{59}Fe] (Figure 2); the rate data in the figure have been corrected for uptake in the negative control. These corrected data were fit to the standard Michaelis−Menten equation; the fitted constants are given in the table (±SEM). The relative values of V_{max}/K_M are with reference to the wild-type Fet3p−Ftr1p complex. NASQ refers to the Ftr1p(D246N/E249Q) mutant. [b] Note that in taking into account the propagation of error in V_{max}/K_M, one-way ANOVA comparison of difference in the WT-WT and E185D-NASQ values yields a P = 0.056.

of effect seen when two otherwise "silent" mutations are combined, which can be quantified in terms of binding energy (Discussion), suggests that, in the binding and trafficking of iron, E185 in Fet3p and the DASE motif in Ftr1p interact. A reasonable explanation for this behavior is that they interact via their simultaneous binding of Fe^{III} in the same state or states along the ferroxidation, permeation pathway.

A concern in comparing V_{max} values for a cellular process involving recombinant, episomally encoded proteins is the relative concentrations of the proteins associated with the process being quantified. We have addressed this issue in our previous work by the use of fluorescent protein fusions of Fet3 and Ftr1 proteins. GFP, YFP, and CFP fusions to Fet3p and Ftr1p are fully wild type in activity and allow visualization by confocal fluorescent microscopy of the fusion proteins' localization to the PM and these proteins'

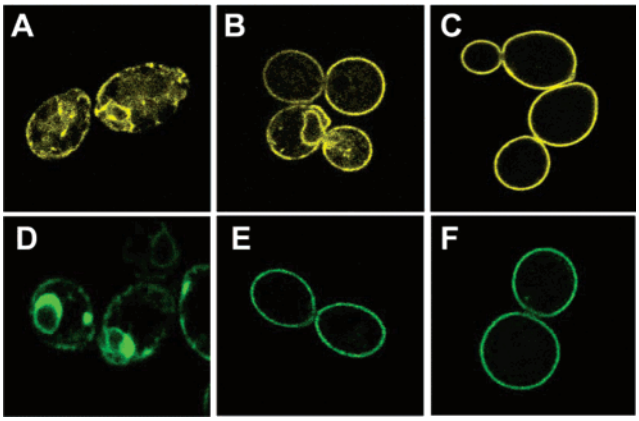

FIGURE 3: Plasma membrane localization of Fet3p, Ftr1p species. Fluorescently tagged fusions of the wild-type and mutant forms of Fet3p and Ftr1p used in these studies were produced in the *fet3*Δ*ftr1*Δ-containing strain, AJS05. These transformants were examined by confocal fluorescent microscopy to ensure the correct plasma membrane targeting of the uptake complex in all cases. These images showed also comparable abundance of the various combinations in the plasma membrane; protein abundance was quantified directly by scanning spectrofluorometric analysis of these cells in suspension (Materials and Methods). The representative samples shown here are as follows: (A) Ftr1:YFP alone (no Fet3p, negative control for complex assembly and targeting); (B) Ftr1:YFP−Fet3p (wild-type positive control); (C) Ftr1(D246N/E249Q):YFP−Fet3p; (D) Fet3:GFP alone (no Ftr1p, negative control); (E) Fet3:GFP−Ftr1p (positive control); (F) Fet3(E185D):GFP−Ftr1p.

quantification by scanning solution fluorescence of cells in suspension (*13*, *25*). Representative confocal images are shown in Figure 3; these demonstrate the correct PM localization of the mutants kinetically characterized in Figure 2 and Table 1. In addition, the fluorescence emission envelopes obtained by scanning spectrofluorometric analysis of cells expressing these several fusion proteins varied by at most 20% (Supporting Information, Figure S1). Both findings support our conclusion that the V_{max} differences determined for uptake complexes containing mutant forms of either or both proteins reflect real differences in activity and not relative abundance or PM localization. K_M values (and K_I values, see later) are concentration-independent constants in this context.

Conditional Citrate Inhibition of Iron Uptake in Fet3p, Ftr1p Trafficking Mutants. These results suggested a corollary, namely, that this less efficient trafficking of iron in ferroxidation and uptake for the double mutant could result in a conditional sensitivity to a ferric iron chelator added exogenously to the ferroxidase−permease complex. Metabolite trapping like this, or lack thereof, is a classic test of a channeling mechanism (*35*, *36*). To test this hypothesis, we first quantified ^{59}Fe uptake by several of these mutant complexes in the presence of citrate as the potential iron chelator. In this experiment, we combined either a mutant Ftr1p with wild-type Fet3p or the inverse; we also examined the citrate effect on iron uptake through a complex in which both proteins carried specific amino acid substitutions. Two types of Ftr1p mutants were used in this screen: those with substitutions in exocytoplasmic domains and those with substitutions in transmembrane ones (cf. Figure 1). The uptake data as a function of [citrate] for complexes containing a single mutant protein are shown in Figure 4A whereas the data for inhibition of uptake through complexes in which both proteins carried mutations are shown in Figure 4B; the

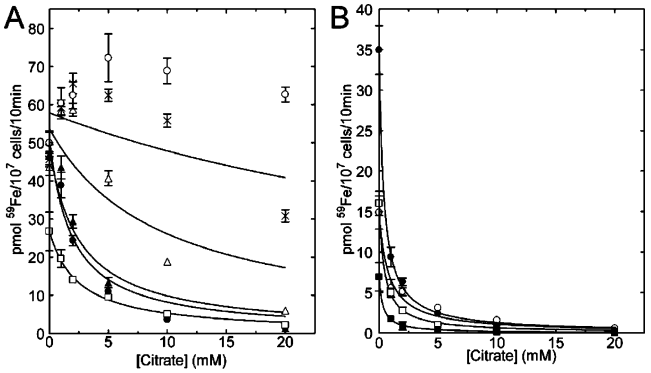

FIGURE 4: Kinetic analysis of citrate inhibition of ^{59}Fe uptake in wild-type and mutant Fet3p−Ftr1p complexes. Reductase-independent ^{59}Fe uptake was carried out as described in Figure 2 with [^{59}Fe] = 0.2 μM ≈ K_M for Fe uptake through the wild-type Fet3p−Ftr1p complex (cf. Table 1). The velocity of uptake was determined as a function of [citrate] as indicated. Wild-type and mutant forms of Fet3p and Ftr1p were produced in the combinations indicated below in the *fet3*Δ*ftr1*Δ-containing strain, AJS05. The raw data (corrected for the negative control) were derived from replicate measurements (n = 3) while the data points and error bars in the figure represent means ± SEM from at least three separate experiments. (A) Data for cells containing either a mutant Fet3p or a mutant Ftr1p in combination with a wild-type partner. The combinations used were as follows (from the least to the most citrate sensitive): Fet3p−Ftr1p, open circles; Fet3p(D409E)−Ftr1p, crosses; Fet3tp(D409A)−Ftr1p, open triangles; Fet3p(D283A)−Ftr1p, filled triangles; Fet3p−Ftr1p(D246N/E249Q), open squares; Fet3p-(E185D)−Ftr1p, filled circles. (B) Data for cells containing Ftr1p-(D246N/E249Q) with the following Fet3p mutants (from the least to the most citrate sensitive): Fet3p(D409E), open circles; Fet3p-(D283A), filled circles; Fet3p(D409A), open squares; Fet3p-(E185D), filled squares.

Table 2: Kinetic Constants for Citrate Inhibition of ^{59}Fe Uptake through Wild-Type and Mutant Fet3p−Ftr1p Complexes

Fet3p−Ftr1p in complex	^{59}Fe uptake (pmol per 10^7 cells per 10 min)[a]	K_I(Cit) (mM)
WT-WT	61.3 ± 0.9	no inhibition[b]
WT-NASQ	26.9 ± 2.4	2.4 ± 0.8
E185D-WT	51.1 ± 2.4	1.9 ± 0.3
D409E-WT	57.9 ± 2.7	48 ± 19[c]
D409A-WT	53.8 ± 3.6	9.4 ± 3.0
D283A-WT	48.7 ± 2.2	2.5 ± 0.4
E185D-NASQ	6.9 ± 0.8	0.3 ± 0.1
D409E-NASQ	14.8 ± 1.1	0.8 ± 0.2
D409A-NASQ	16.0 ± 0.7	0.4 ± 0.1
D283A-NASQ	35.0 ± 1.4	0.4 ± 0.1

[a] Uptake values obtained at [^{59}Fe] = 0.2 μM, ~K_M for iron. [b] At maximum [citrate] used (20 mM). [c] K_I value > [citrate] used (≤20 mM), reducing significance of fitted value.

smooth curves represent fits of these data to eq 1 (Materials and Methods), an equation that describes simple competitive inhibition of Fe uptake by the added iron chelator.

The results of this kinetic structure−function analysis can be described as follows. First, with respect to the uptake velocity at 0.2 μM ^{59}Fe^{II} in the absence of citrate (the ordinate axis values in Figure 4,B and values in Table 2, first column), the mutant complexes fall into four broad classes. The first is those exhibiting wild-type activity, Fet3p(E185D), Fet3p-(D409E), Fet3p(D409A), and Fet3p(D283A). The second is those with 25−50% wild-type activity, including Ftr1p-(NASQ) and the Fet3p(D409A), Fet3p(D409E), and Fet3p-(D283A) mutants with Ftr1p(NASQ). The third is the double mutant complex, Fet3p(E185D)−Ftr1p(NASQ), that exhibited <10% wild-type uptake activity at this [^{59}Fe], a fact that reflected the smaller V_{max}/K_M for this double mutant species. This latter kinetic behavior was analyzed in more detail above (Figure 2 and Table 1). The fourth group is complexes in which wild-type Fet3p was combined with Ftr1 proteins carrying E → D substitutions in either one or both of the essential REXLE motifs found in transmembrane domains 1 and 4 (Figure 1 and ref *13*). These mutant Ftr1 proteins exhibit 20−50% wild-type uptake activity (*13*) but, like wild type, were insensitive to citrate (data not shown). This result indicates that citrate sensitivity is not due to impaired iron permeation through Ftr1p per se; rather, this sensitivity appears to result only from mutations in the exocellular domains of the ferroxidase, permease proteins.

Second, the data overall do fit to a simple competitive inhibition kinetic scheme indicating that this is the kinetic mechanism by which citrate inhibits uptake at a constant [^{59}-Fe]. These fitted K_I values for citrate are given in Table 2, second column. Third, with respect to their sensitivity to this inhibition by citrate [the relative K_I(Cit) values], the mutants again fall into three classes: the Fet3p(D409E) complex was wild type in that it was very weakly inhibited by citrate (if at all); the Fet3p(D409A) complex was moderately sensitive to citrate; and the remainder of the uptake species were 4−30-fold more sensitive than was the ferroxidase−permease complex containing this latter Fet3p mutant. There was an overall correlation between the members of the groups distinguished by effects on uptake velocity at [^{59}Fe] = 0.2 μM and by effects on K_I. There also was marked synergism evident in two of the K_I values, those for the Fet3p(D409A) and Fet3p(D409E) mutants; uptake complexes containing either of these two Fet3p mutants and Ftr1p(NASQ) were 24- and 60-fold more sensitive to citrate, respectively, than the corresponding complexes assembled with wild-type Ftr1p.

Chelator Strength and ^{59}Fe Uptake Inhibition: A Thermodynamic Test of the Mechanism of Inhibition. There are two simple models for how a ferric iron chelator like citrate could inhibit the uptake by Ftr1p of the Fe^{III} generated by Fet3p; these two schemes are illustrated in Figure 5A. In the first, dissociative kinetic Scheme 1, the Fet3p-generated Fe^{III} diffuses into bulk solvent and there equilibrates with the chelator and the Fe(III)·chelator complex. In this model in which Fe^{III} dissociation is kinetically fast compared to Fe^{III} permeation through Ftr1p, the K_I value for inhibition should correlate with the stability of the Fe(III)·chelate complex. In this rapid equilibrium condition, a 10-fold increase in chelator strength should, in the limit, correlate with a 10-fold decrease in K_I (denoting more efficient inhibition).[2] Scheme 2 (the other limiting model) is an associative one in which rather than the Fe^{III} dissociating into bulk solvent, the chelator associates with the Fet3p−Ftr1p complex in some fashion so as to block iron trafficking, perhaps by scavenging the Fe^{III} via a series of ligand exchange reactions. This second model has as its essential element the channeling of Fe^{III} in the complex; this kinetic

[2] At face value, the data (and fits) shown in Figure 4 preclude this mechanism since in it the chelator would be acting to deplete the substrate (Fe^{III}) for the second step in the pathway reaction being measured, i.e., iron uptake. The equation relating velocity to [inhibitor] for substrate depletion is quadratic in form, not the hyperbolic, competitive inhibition function that the data appear to fit (*26*).

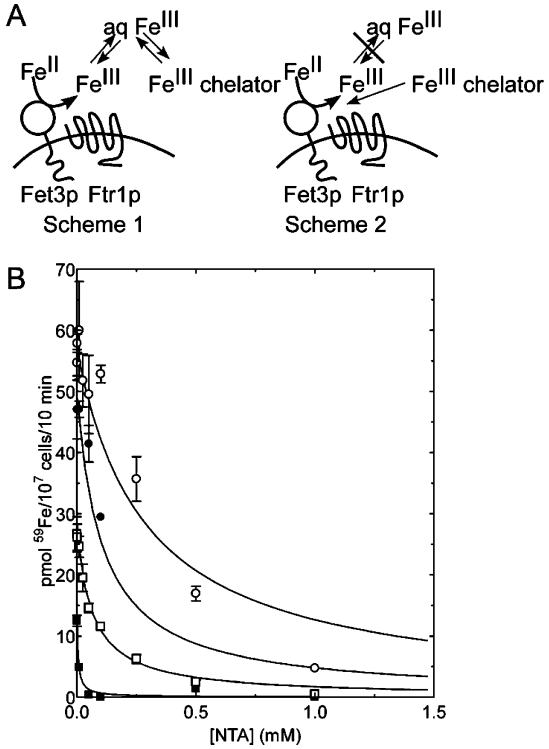

FIGURE 5: A test of channeling: correlating Fe(III)·chelate stability with ^{59}Fe uptake inhibition. (A) Scheme 1 diagrams a dissociative mechanism of Fe trafficking between Fet3p and Ftr1p in Fe uptake via the permease complex. In this mechanism, Fet3p-produced Fe^{III} equilibrates with the bulk phase from which it can be trapped by an added ferric iron chelator. Scheme 2 diagrams a strict channeling mechanism of Fe trafficking in which the transfer of Fe^{III} from one protein to the other is nondissociative and occurs as a result of a series of ligand exchange reactions. In this case, an added chelator can only inhibit Fe uptake by scavenging Fe^{III} out of the complex, a kinetically rather than thermodynamically controlled process. Therefore, while inhibition of Fe uptake occurring by Scheme 1 would correlate with chelator strength, inhibition of Fe uptake occurring by Scheme 2 would likely not. (B) Inhibition of ^{59}Fe uptake quantified as described in this figure is given as a function of [NTA] as indicated. The AJS05 strain contained the following combinations of Fet3p, Ftr1p species: Fet3p−Ftr1p, open circles; Fet3p(E185D)−Ftr1p, filled circles; Fet3p−Ftr1p(NASQ), open squares; Fet3p(E185D)−Ftr1p(NASQ), filled squares.

mechanism of iron trafficking could be termed nondissociative to emphasize this feature. A third model is one in which Fe^{III} dissociation occurs but competes weakly with trafficking/permeation, or $k_{off} \ll k_{permeation}$. The second and third models do not of necessity predict the strict linear free energy relationship between chelator strength and inhibition constant that the first one does since in these latter two models access to the Fet3p-generated Fe^{III} is kinetically and not thermodynamically controlled. We used nitrilotriacetate (NTA) and hydroxyethylenediaminetriacetic acid (HEDTA) as additional Fe^{III} chelators to assess the type of correlation the Fet3p−Ftr1p system exhibited in regard to chelator strength.

NTA complexes with Fe^{III} with log $K_1 = 15$; this value compares to the ferric citrate complex that has log $K_1 = 10$ (values at pH = 6.0) (*37*). In other words, Scheme 1 would predict that NTA would have an effect on Fe uptake that could be as much as 10^5 times more robust than that measured for citrate. The results for inhibition by NTA of the Fe uptake through the wild-type and mutant Fet3p−Ftr1p complexes kinetically characterized in Figure 2 and Table 1 are given in Figure 5B, with the fitted K_I values included in Table 3, second data column. Analysis of these data clearly showed that NTA is a considerably more effective inhibitor of reductase-independent ^{59}Fe uptake than is citrate. For example, NTA inhibited uptake through the wild-type complex with a $K_I = 287$ μM (open circles; citrate was without effect on this complex) and through the Ftr1p-(NASQ)-containing complex with a $K_I = 69$ μM (open squares; compare to $K_I = 2.4$ mM for citrate, values repeated in Table 3). The stronger inhibition by NTA of ^{59}Fe uptake through all four Fet3p−Ftr1p forms could be consistent with either kinetic Scheme 1 or Scheme 2. Clearly, however, the nearly 10^5-fold greater stability of the ferric−NTA complex in comparison to the ferric−citrate one is not reflected quantitatively in the 20−40-fold increase in inhibition of uptake through any of the Fet3p, Ftr1p species examined (Table 3, compare second to first data columns). Similarly, the simple dissociative mechanism of iron trafficking would predict an HEDTA-dependent inhibition that reflected the log $K_1 = 19$ for the corresponding ferric iron complex. The fitted K_I values for HEDTA inhibition (Table 3, third column) show instead that they correspond to a relatively modest ~70-fold more efficient inhibition than that observed with NTA; indeed, the double mutant-containing complex was only 14-fold more sensitive to HEDTA than to NTA. Qualitatively, this pattern suggests a correlation between chelator strength and inhibition that is relatively weak thermodynamically. This correlation in turn suggests a mechanism of inhibition in which only a small fraction of the binding energy released upon Fe·chelate formation is coupled to the trapping of Fe^{III} from the permeation pathway.

Table 3: Fe^{III}·Chelator Inhibition Constants of ^{59}Fe Uptake through Wild-Type and Mutant Fet3p−Ftr1p Complexes[a]

Fet3p−Ftr1p in complex	K_I(Cit) (mM)[b]	K_I (NTA) (μM)[b]	K_I(HEDTA) (μM)[b]	inhibition β[c]
WT-WT	none fitted	287 ± 53	3.6 ± 0.8	−0.46 ± 0.02
WT-NASQ	2.4 ± 0.8	69 ± 23	1.0 ± 0.1	−0.36 ± 0.04
E185D-WT	1.9 ± 0.3	106 ± 24	1.2 ± 0.4	−0.35 ± 0.06
E185D-NASQ	0.3 ± 0.1	7 ± 1	0.5 ± 0.5[d]	−0.32 ± 0.02

[a] Values obtained at [^{59}Fe] = 0.2 μM, ~K_M for iron. [b] Note difference in units for citrate versus NTA and HEDTA K_I values. [c] Values derived from linear least-squares fit of data in Figure 6. For the purposes of this analysis, the K_I(Cit) for WT-WT was assumed to be 50 mM. [d] Limiting uptake rate introduced large standard error.

This correlation was demonstrated analytically in a standard rate, equilibrium linear free energy plot (Figure 6). The slopes of the fitted lines are equivalent to an inhibition β-value; these values are given in Table 3, also (last column). Clearly, there is a linear correlation between log K_I and log K_1 with β-values for the four complexes that fall on either side of −0.36. Empirically, this value means that K_I decreased by a factor of 10 as the stability constant, K_1, increased by 10^3. This behavior is inconsistent with a strict equilibrium, dissociative model of Fe trafficking in the Fet3p−Ftr1p complex (Scheme 1) but can be rationalized in terms of either of the other models outlined above (see also Discussion). The plots also highlight the convergence of the K_I values to ~1 μM, suggesting that a kinetic step(s) in the trafficking/permeation and/or inhibition pathways limit(s) partitioning between the two; this convergence is reflected also in the systematic decrease in the absolute value of the slope (β) in going from the wild-type complex to the one containing the Fet3(E185D)−Ftr1(NASQ) proteins.

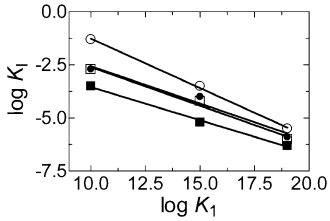

FIGURE 6: Linear correlation between log K_I and log K_1. Fitted values of K_I from kinetic data as in Figures 4 and 5 (for citrate and NTA) and for HEDTA (data not shown) are plotted against the log K_1 values for the corresponding chelator·Fe^{III} complexes (10, 15, and 19, respectively). The lines are derived from a linear least-squares fit; the slopes and their standard errors are given in Table 3. The K_I values are for the following combinations of Fet3p, Ftr1p species: Fet3p−Ftr1p, open circles; Fet3p(E185D)−Ftr1p, filled circles; Fet3p−Ftr1p(NASQ), open squares; Fet3p(E185D)−Ftr1p-(NASQ), filled squares. For the purposes of this analysis, the K_I value for citrate inhibition of the wild-type complex was assumed to be 50 mM.

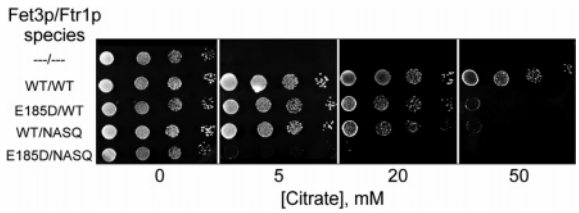

FIGURE 7: Citrate sensitivity correlates with a conditional inhibition of respiratory (iron-requiring) growth. Serial dilutions of cultures of the *fet3*Δ*ftr1*Δ-containing strain, AJS05, producing wild-type or mutant forms of Fet3p and Ftr1p were spotted onto solid media without or with added citrate; the culture identity with respect to the Fet3 and Ftr1 proteins and the citrate concentrations are indicated in the figure. Glycerol was the nonfermentable carbon source used in the yeast extract, peptone-containing (YP) media. The plates were imaged following 4 days of growth.

Citrate-Sensitive Iron Uptake Complexes Correlate with Citrate-Sensitive Growth. The tight coupling of ferroxidation and permeation indicated by the citrate insensitivity of the wild-type Fet3p−Ftr1p complex would appear to offer a selective growth advantage over a strain producing an iron uptake complex leaky with respect to added iron chelator. This inference was tested directly by examination of the growth of yeast strains deficient in the complex altogether or producing either wild-type or mutant forms of either or both proteins. The high-affinity iron uptake function in yeast correlates physiologically with respiratory (iron-requiring) growth on a nonfermentable carbon source like glycerol (*11*, *38*). As shown in Figure 7, the citrate sensitivity of respiratory growth correlated well with the citrate sensitivity of the complex produced in a specific yeast strain (compare to Figure 4 and Tables 2 and 3). Whereas the wild-type complex was capable of supporting growth at 50 mM citrate, growth of strains producing a complex containing either Fet3p(E185D) or Ftr1p(NASQ) was inhibited. The strain producing the double mutant complex failed to grow at all at 5 μM citrate and, in fact, exhibited a growth phenotype little different from the negative control, the parental *fet3*Δ*ftr1*Δ-containing strain, AJS05.

^{59}Fe Uptake by Fet3p, Ftr1p Chimeras and Their Citrate Sensitivity. Our studies were initiated with the knowledge that exogenously added or produced Fe^{III} was not the substrate for iron permeation by Ftr1p. The fact that such ferric iron was not the substrate for uptake was consistent with but far from definitive evidence for a channeling model of iron trafficking in the Fet3p−Ftr1p complex. We have now made use of a test of channeling, metabolite trapping, and have quantified the kinetic access to Fet3p-generated Fe^{III} by iron chelators. Another strategy used as a probe of channeling in a coupled, metabolic pathway is to dissect the pathway steps by protein engineering. Thus, we took the wild-type, two-component ferroxidase−permease system and from it constructed a bifunctional protein in which the soluble, Fet3p MCO domain (residues 1−555) was tethered to the exocytoplasmic amino terminus of Ftr1p. Two such chimeric genes were constructed that differed in the linker length encoded between the two ORFs; in one, the length was 11 residues (designated C1); in the other it was 29 residues (designated C2). Note also that the predicted sequence length between the exocytoplasmic domain−plasma membrane surface associated with the first, amino-terminal transmembrane element in Ftr1p and the MCO core of Fet3p (assumed to include up to Fet3p residue 500) was 63 residues in addition to the linker used in the construction a given chimera (Materials and Methods). In other words, the effective linker lengths in C1 and C2 were 74 and 92 residues, respectively. These chimeras were produced in a *fet3*Δ*ftr1*Δ strain along with the ferroxidase-negative Fet3p-(T1D) to act as a protein chaperone for the trafficking of the chimera. This engineered uptake complex is illustrated by Scheme 3 in Figure 8A.

We first demonstrated that our Fet3pMCO:Ftr1p fusions assembled in the PM along with the ferroxidase-negative Fet3p(T1D); we did so using GFP-tagged versions of the chimeras. As demonstrated by the confocal fluorescence microscopic images shown in Figure 8B, C1 trafficked to the plasma membrane with either wild-type Fet3p (A) or Fet3p(T1D) (B) as did C2 (panels C and D of Figure 8B, respectively); as is the case with Ftr1p (*13*, *25*), both chimeras remained in the perinuclear space when produced in the absence of any Fet3p species at all (not shown). These data indicate that these fusions were wild type with respect to complex assembly and plasma membrane targeting. We then performed kinetic analyses of ^{59}Fe uptake via these Fet3p-(T1D)−Fet3pMCO:Ftr1p complexes as a function of [citrate] as in Figure 4. These citrate inhibition data are shown in Figure 9.

The data show that both chimeras behaved much like Fet3p(E185D) in complex with Ftr1p: at [^{59}Fe] = 0.2 μM (approximate V_{max}/K_M conditions) and in the absence of citrate, C1 (filled circles) and C2 (open circles) supported uptake that was ∼85% of wild type (56 ± 4 and 49 ± 3 pmol of ^{59}Fe per 10 min per 10^7 cells, respectively) but were inhibited by citrate with K_I values of 2.8 ± 0.7 and 2.1 ± 0.5 mM (values from fits to eq 1). Thus, with respect to sensitivity to citrate, the chimeras were similar to other trafficking mutant complexes including the ones containing Fet3p(D283A) and Ftr1p(NASQ) (Table 2). Introduction into C1 of the Fet3p:MCO substitution E185D (open triangles) or the Ftr1p ^{246}NASQ^{249} substitution (open squares) reduced the efficiency of this chimera in ^{59}Fe uptake by ∼50% (to 26 ± 2 and 21 ± 2 pmol of ^{59}Fe per 10 min per 10^7 cells, respectively). These mutant chimeras also were more citrate sensitive with K_I values of 0.14 ± 0.06 and 0.69 ± 0.18 mM, values that were comparable to the double mutant containing, Fet3p, Ftr1p heterooligomeric complexes (Table

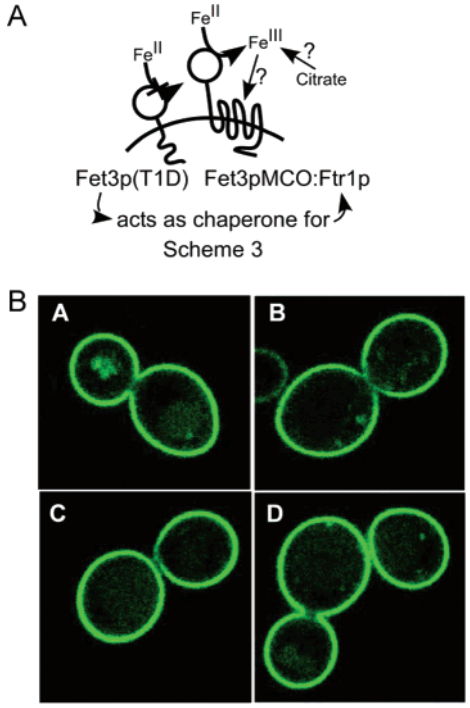

FIGURE 8: Fet3pMCO:Ftr1p fusions are localized to the yeast plasma membrane. Scheme 3 illustrates that the chimeras require a ferroxidase-negative, Fet3p(T1D) protein acting as chaperone for complex assembly and targeting of the chimera to the plasma membrane. GFP fusions of chimeras C1 (panels A and B) and C2 (panels C and D) were produced in the *fet3*Δ*ftr1*Δ-containing strain, AJS05, along with either wild-type Fet3p (panels A and C, respectively) or the ferroxidase-negative mutant, Fet3p(T1D) (panels B and D, respectively). The cells were imaged by confocal fluorescence microscopy as shown. In the absence of the coproduction of the Fet3p(T1D) required to assemble with and chaperone the chimeras to the plasma membrane, these fluorescent fusions remained in the perinuclear regions of the cells (negative control not shown).

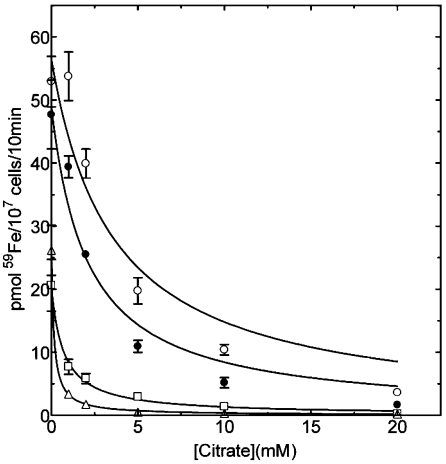

FIGURE 9: Kinetic analysis of citrate inhibition of ^{59}Fe uptake through Fet3pMCO:Ftr1p fusions. The [citrate] dependence of ^{59}Fe uptake was measured and analyzed as in Figure 4 in strain AJS05 producing the Fet3pMCO:Ftr1p fusions as indicated along with ferroxidase-negative Fet3p(T1D) as protein chaperone for the chimera. The samples are as follows: C1 wild type, open circles; C2 wild type, closed circles; C1[Ftr1p(NASQ)], open squares; C1-[Fet3pMCO(E185D)], open triangles.

2). In summary, a bifunctional iron uptake protein can be as efficient as the wild-type two-component one but exhibits a metabolic leakiness not seen in the latter complex. This structure−function correlation more closely follows from an associative, channeling mechanism for the wild-type system (Scheme 2, Figure 5) than it does from the alternative dissociative model of Fe trafficking (Scheme 1, Figure 5). Fe trafficking via this latter model reasonably would be indifferent to the precise conformational relationship of the ferroxidase and permease functional sites.

DISCUSSION

Metabolite channeling in which the product of a proximal activity in a metabolic pathway traffics as substrate to a distal activity without equilibration with bulk solvent is an inherently efficient kinetic process since it eliminates the concentration-dependent second-order binding of solutes derived from solvent (*36*, *39*). Channeling requires the close proximity of the donor and acceptor sites. This proximity can be enforced by close packing (crowding) of the proximal and distal proteins (as is often likely in vivo) (*40*), by the formation of a specific complex between the two proteins (*39*, *41*), or by the gene splicing that encodes the donor and acceptor sites in the same gene as for a bifunctional enzyme (*42*). If the Fet3p−Ftr1p system supports channeling, this mechanism would rely in part on the fact that the two proteins are part of a heterodimeric, two-component complex (at the least) in the yeast plasma membrane (*11*, *13*).

Channeling is chemically efficient as well since it does, in effect, restrict the reaction coordinate available to the product of the proximal step. By directing this species to the distal site, channeling prevents the possible side reactions that would decrease the overall yield of the pathway. The hydrolysis of Fe^{III} would certainly represent one such side reaction competing with Fe^{III} permeation if the ferric iron produced by Fet3p were to equilibrate with bulk water. A channeling mechanism for Fet3p−Ftr1p would appear to avoid a futile cycle of ferrireduction (and mobilization) followed by ferroxidation but with hydrolysis (rather than uptake); this ferric hydroxide would need rereduction if it were to be a substrate for the Fet3p−Ftr1p complex. A channeling mechanism for Fe^{III} trafficking in the Fet3p−Ftr1p system is therefore teleologically sound on a chemical basis and is physically possible given the fact that these two proteins are associated in the yeast plasma membrane (*13*). We have provided data here that strongly support this kinetic model for iron uptake through the Fet3p−Ftr1p complex.

As noted in the introduction, iron channeling in this complex could be inferred from the fact that exogenous Fe^{III} is not substrate for iron permeation; this behavior for ferric iron is in contrast to that for ferrous iron that is taken into the cell via Fet3p−Ftr1p, by-passing the ferrireductase, Fre1p (*7*, *9*). Here, however, we have shown that the Fet3p MCO (ferroxidase) domain when tethered to the Ftr1p permease in the exocytoplasmic space efficiently supplies the Fe^{III} for uptake. This experiment by itself also fails to provide explicit evidence in favor of a channeling mechanism of iron trafficking (e.g., evidence in favor of Scheme 2) although the difference in citrate sensitivity of the two Fet3pMCO:Ftr1p chimeras in comparison to wild type did indicate that the ferroxidase activity of the chimera alone was not sufficient to support wild-type iron permeation.

Our use of Fe^{III} chelators to distinguish between Schemes 1 and 2 via kinetic analysis mirrors the use of Mg^{II} as inhibitor of the coupled aldolase−fructose 1,6-bisphosphatase

(FBPase) reactions. Rakus et al. demonstrated that these two glycolytic enzymes associate and that the flux through this two-step reaction was activated by the two enzymes functioning as an enzyme complex, certainly a corollary to the selective advantage of a channeling mechanism (*41*). The authors took advantage of the fact that Mg^{II} inhibits the FBPase reaction itself by sequestering the substrate for it, fructose 1,6-bisphosphate (F1,6-P_2). In the coupled reaction catalyzed by the aldolase−FBPase complex, however, inhibition by Mg^{II} was strongly reduced, indicating that the F1,6-P_2 produced by aldolase in this complex did not equilibrate with bulk solvent where it would chelate and effectively be trapped by the Mg^{II}. The Fet3p−Ftr1p system here is different only in that the metal ion is the intermediate in this permeation pathway, and it is the metal ion being trapped by the chelating agent rather than the reverse.

What our iron permeation pathway did not provide, however, was the negative control for channeling represented by the isolated FBPase reaction that is demonstrably inhibited by Mg^{II} (*41*). However, we were able to generate this negative control *conditionally* in that some mutant forms of Fet3p and of Ftr1p proved to be "leaky" with respect to the inhibitory effect of an added Fe^{III} chelator. Although not as well characterized kinetically as our mutants here were, a similar kind of leakiness has been inferred genetically in the ferrochelatase reaction in *Bacillus subtilis* (*43*) and in the incorporation of UDP-D-galactose into cell wall polysaccharides in *Arabidopsis* (*44*). In both of those cases, the phenotypes associated with specific mutations were seen as the result of a decline in the efficacy of channeling in the respective pathways. We propose that the citrate inhibition observed in an Ftr1p(NASQ)-containing complex, for example, indicates that channeling occurs in the wild-type one that itself is indifferent to the presence of this chelating agent. The growth phenotypes of yeast producing wild type in comparison to citrate-sensitive mutant Fet3p−Ftr1p complexes demonstrate that this "indifference" does provide a selective growth advantage.

There are two results with these mutants that most strongly support (although do not prove) a channeling mechanism in the Fet3p−Ftr1p system (Figure 5, Scheme 2). First is the functional interaction between a side chain in Fet3p and one in Ftr1p in iron trafficking as indicated by the synergism in mutagenic effects in a double mutant complex. One example of this is the reduced uptake velocity for the Fet3p(E185D)−Ftr1p(NASQ) complex at 0.2 μM ^{59}Fe; this value, 6.9 pmol of ^{59}Fe per 10 min per 10^7 cells, is ~10% of wild type (Table 2). This difference in velocity is worth ~1.5 kcal/mol in activation energy. The single mutant, Fet3p(E185D), is wild type in uptake activity. The other single mutant, Ftr1p(NASQ), is less efficient by a factor of ~2 (Table 2), representing a loss of ~0.4 kcal/mol binding energy in some state essential to iron permeation. This analysis suggests that in a heterooligomeric complex containing a single mutation on each monomer there is an additional ~1 kcal/mol of binding energy lost in the activation of iron trafficking due, most reasonably, to the loss of an interaction between E185 in Fet3p (due to the E185D substitution) and the ^{246}DASE^{249} motif in Ftr1p (due to the substitution of NASQ), an interaction that is coupled to iron trafficking. This double-mutant effect has been well recognized in comparable reverse genetic approaches to the elucidation of protein−ligand interactions, protein folding, and enzyme mechanism, building upon the well-established relationships between state changes and binding energies (*31*−*34*, *45*). Note, however, that the kinetic differences exhibited by the wild-type and single mutant in comparison to the double mutant complexes were statistically marginal; the interaction energy inferred above suffers from the same limitation. Nonetheless, the behavior of the v versus [^{59}Fe] and the chelator inhibition data do suggest that the overall efficacy of a double mutant complex is compromised in comparison to the "sum" of the activities of the corresponding single mutant ones irrespective of the extent to which the precision of the data allows us to quantify the difference.

The second observation consistent with a channeling mechanism (Scheme 2) is the weak thermodynamic coupling of inhibitor strength (given by its log K_I value) and chelator strength (given by its log K_1 one). If the chelator were trapping Fe^{III} in thermodynamic (rapid) equilibrium with the bulk phase (Scheme 1), our kinetically determined K_I values should exhibit a relatively strong dependence on the stability constant values for the three ferric iron chelators used. In fact, the Brønsted values for the wild-type and three mutant complexes ($\beta = -0.32$ to -0.46) show that the coupling of chelate stability to the trajectory of Fe^{III}-trafficking inhibition is relatively weak; e.g., for the two single mutant complexes, a 10^3 increase in K_1 results in only a 10-fold decrease in K_I.

This weak coupling between chelator strength and inhibitory effect could reflect a mechanism(s) other than the simple channeling one we have discussed which is contrasted with an *equilibrium* model of Fe trafficking (Scheme 2 versus Scheme 1). The weakness of the argument above is that it *assumes* inhibition is thermodynamically rather than kinetically controlled. An alternative model in which Fe^{III} equilibrates with solvent slowly relative to continued trafficking in the complex is consistent with the relatively weak effect increased chelator strength has on the inhibition observed. This situation is functionally equivalent to $K_{stab}^{protein} \gg K_{stab}^{chelator}$ with respect to Fe^{III} binding. Note, however, that tight binding is nearly always due to a kinetically limiting rate constant for dissociation of the ligand from the pathway protein(s) (*26*). Thus, tight binding of Fe^{III} in the Fet3p−Ftr1p system is equivalent to a kinetic scheme in which dissociation of Fet3p−Ftr1p-bound Fe^{III} competes poorly with downstream permeation steps. A mechanism like this one would function physiologically in lieu of a strict channeling one; our data are compatible with either model.

Copper trafficking in yeast and higher eukaryotes provides an appropriate analogy to the model suggested here for the Fet3p−Ftr1p high-affinity iron uptake system. Copper trafficking starts with the high-affinity, plasma membrane Cu^I transporter, Ctr1p, and includes the copper chaperone, Atx1p in yeast (Atox1/HAH1 in humans), and the Cu-ATPase, Ccc2p in yeast (ATP7A or ATP7B in humans) (*46*). In vitro studies suggest that Cu^I translocated by Ctr1p exchanges into Axt1p at the cytoplasmic face of the plasma membrane (*47*, *48*). This Atx1p copper subsequently exchanges into the Ccc2p Cu-ATPase that is located in the membrane of a Golgi or post-Golgi compartment; this Cu pump concentrates the copper in the lumen of this compartment where it is available for the metalation of apo-Fet3p (for example) (*46*). The transfer of Cu^I from Atx1 to Ccc2 is, like the first trafficking step in this copper metabolic pathway, mechanistically

nondissociative in nature (*49*). This copper channeling is critical to maintaining a diminishingly small level of "free" copper in the yeast cell as a means of protecting the cell from this metal ion's prooxidant behavior (*50*). Iron is no less an effective prooxidant; thus, in addition to preventing hydrolysis, iron channeling can have a cytoprotective effect as well.

Channeling appears to be a common feature of bifunctional enzymes, and topologic channels or tunnels have been structurally characterized by X-ray crystallography in some cases (*39*, *51*). Acetyl-CoA synthase is a classic example of this pattern in which the CO product from the carbon dioxide reductase active site migrates through the protein to the synthase site where the CO is used to assemble the acetyl group (*52*, *53*). We may have engineered a bifunctional form of the yeast high-affinity iron uptake complex with our Fet3p MCO, Ftr1p chimera. Certainly, both chimeras, when "chaperoned" to the plasma membrane with an inactive form of Fet3p, supported wild-type iron uptake. However, neither chimera was wild type with respect to iron channeling as indicated by its sensitivity to citrate; as noted, in this respect, both were comparable to some of the two-component, Fe trafficking mutant complexes. A more subtle difference was observed in the C1 chimera carrying the Fet3p E185D mutation in comparison to the Ftr1p NASQ substitution. In the normal Fet3p−Ftr1p complex these mutations result in essentially the same citrate sensitivity ($K_I \approx 2$ mM). In contrast, for the mutant C1 proteins, these K_I values differ by 5-fold (0.14 versus 0.69 mM, respectively). This suggests that the role played by these two side chains in Fe trafficking is conformation-dependent, an inference more compatible with an associative, channeling mechanism for this process.

When Stearman and co-workers identified Ftr1p as the permease that supported high-affinity iron uptake in yeast, they noted the presence of EXXE motifs in both transmembrane and carboxyl-terminal domains (cf. Figure 1) (*11*). They compared these motifs to the DXXE motif that lines the so-called 3-fold channels that connect the ferritin core to the outside surface of the heavy and light chain heteropolymer (*54*). These D and E residues are essential to the channeling of the Fe^{II} into the ferritin core for its ferroxidation (or oxidation) concurrent with its core deposition. H and L chains contain an additional, but not identical, glutamate-rich motif. In H chains, a ^{62}EEREH^{66} sequence is a major part of the ferroxidase site that is unique to these chains (*55*). Theil and co-workers have begun to use protein engineering as we have done here to map out the protein channel associated with this ferroxidase center that funnels iron, as Fe^{II}, from the ferritin pores to the mineral cavity, as Fe^{III} (*56*). The analogy to the Fe^{II} oxidation, Fe^{III} channeling proposed here for the Fet3p−Ftr1p complex is striking and indicates that this mechanism likely represents a conserved aspect of iron homeostasis in aerobic organisms.

ACKNOWLEDGMENT

We thank Dr. Wade Sigurdson for invaluable assistance in the use of confocal fluorescent microscopy to analyze the targeting of the Fet3p−Ftr1p complex to the yeast plasma membrane. We also thank Mr. Thomas Hohle for assistance in the analysis of the citrate sensitivity of respiratory growth (Figure 7).

SUPPORTING INFORMATION AVAILABLE

Quantitative scanning fluorescence emission envelopes from cells producing GFP and YFP fusions of wild-type and mutant forms of Fet3p and Ftr1p demonstrating equal protein production. This material is available free of charge via the Internet at http://pubs.acs.org.

REFERENCES

1. Andrews, N. C., Fleming, M. D., and Gunshin, H. (1999) Iron transport across biologic membranes, *Nutr. Rev. 57*, 114−123.
2. Frieden, E., and Osaki, S. (1974) Ferroxidases and ferrireductases: their role in iron metabolism, *Adv. Exp. Med. Biol. 48*, 235−265.
3. Kosman, D. J. (2003) The molecular mechanisms of iron uptake in fungi, *Mol. Microbiol. 47*, 1185−1197.
4. Bondy, S. C., Guo-Ross, S. X., and Truong, A. T. (1998) Promotion of transition metal-induced reactive oxygen species formation by β-amyloid, *Brain Res. 799*, 91−96.
5. Pierre, J. L., and Fontecave, M. (1999) Iron and activated oxygen species in biology: the basic chemistry, *BioMetals 12*, 195−199.
6. Martins, L. J., Jensen, L. T., Simon, J. R., Keller, G. L., and Winge, D. R. (1998) Metalloregulation of *FRE1* and *FRE2* homologs in *Saccharomyces cerevisiae*, *J. Biol. Chem. 273*, 23716−23721.
7. Dancis, A., Roman, D. G., Anderson, G. J., Hinnebusch, A. G., and Klausner, R. D. (1992) Ferric reductase of *Saccharomyces cerevisiae*: Molecular characterization, role in iron uptake and transcriptional control by iron, *Proc. Natl. Acad. Sci. U.S.A. 89*, 3869−3873.
8. Georgatsou, E., and Alexandraki, D. (1999) Regulated expression of the *Saccharomyces cerevisia*e Fre1p/Fre2p Fe/Cu reductase related genes, *Yeast 15*, 573−584.
9. Hassett, R., and Kosman, D. J. (1995) Evidence for Cu(II) reduction as a component of copper uptake by *Saccharomyces cerevisiae*, *J. Biol. Chem. 270*, 128−134.
10. de Silva, D. M., Askwith, C. C., Eide, D., and Kaplan, J. (1995) The *FET3* gene product required for high affinity iron transport in yeast is a cell surface ferroxidase, *J. Biol. Chem. 270*, 1098−1101.
11. Stearman, R., Yuan, D. S., Yamaguchi-Iwai, Y., Klausner, R. D., and Dancis, A. (1996) A permease-oxidase complex involved in high-affinity iron uptake in yeast, *Science 271*, 1552−1557.
12. Yuan, D. S., Dancis, A., and Klausner, R. D. (1997) Restriction of copper export in *Saccharomyces cerevisiae* to a late Golgi or post-Golgi compartment in the secretory pathway, *J. Biol. Chem. 272*, 25787−25793.
13. Severance, S., Chakraborty, S., and Kosman, D. J. (2004) Structure and function in the Ftr1 protein from *Saccharomyces cerevisiae*: orientation, topology and iron permeation residues, *Biochem. J. 380*, 487−496.
14. Solomon, E. I., Sundaram, U. M., and Machonkin, T. E. (1996) Multicopper oxidases and oxygenases, *Chem. Rev. 96*, 2563−2605.
15. Kosman, D. J. (2002) Fet3p, ceruloplasmin, and the role of copper in iron metabolism, in *Advances in Protein Chemistry* (Valentine, J. S., and Gralla, E., Eds.) pp 221−269, Elsevier, New York.
16. Harris, Z. L., Durley, A. P., Man, T. K., and Gitlin, J. D. (1999) Targeted gene disruption reveals an essential role for ceruloplasmin in cellular iron efflux, *Proc. Natl. Acad. Sci. U.S.A. 96*, 10812−10817.
17. Vulpe, C. D., Kuo, Y. M., Murphy, T. L., Cowley, L., Askwith, C., Libina, N., Gitschier, J., and Anderson, G. J. (1999) Hephaestin, a ceruloplasmin homologue implicated in intestinal iron transport, is defective in the *sla* mouse, *Nat. Genet. 21*, 195−199.
18. de Silva, D., Davis-Kaplan, S., Fergestad, J., and Kaplan, J. (1997) Purification and characterization of Fet3 protein, a yeast homologue of ceruloplasmin, *J. Biol. Chem. 272*, 14208−14213.
19. Hassett, R. F., Yuan, D. S., and Kosman, D. J. (1998) Spectral and kinetic properties of the Fet3 protein from *Saccharomyces cerevisiae*, a multinuclear copper ferroxidase enzyme, *J. Biol. Chem. 273*, 23274−23282.
20. Blackburn, N. J., Ralle, M., Hassett, R., and Kosman, D. J. (2000) Spectroscopic analysis of the trinuclear cluster in the Fet3 protein from yeast, a multinuclear copper oxidase, *Biochemistry 39*, 2316−2324.

21. Machonkin, T. E., Quintanar, L., Palmer, A. E., Hassett, R., Severance, S., Kosman, D. J., and Solomon, E. I. (2001) Spectroscopy and reactivity of the type 1 copper site in Fet3p from *Saccharomyces cerevisiae*: correlation of structure with reactivity in the multicopper oxidases, *J. Am. Chem. Soc. 123*, 5507−5517.
22. Palmer, A. E., Quintanar, L., Severance, S., Wang, T.-Z., Kosman, D. J., and Solomon, E. I. (2002) Spectroscopic characterization and O_2 reactivity of the trinuclear cluster of mutants of the multicopper oxidase Fet3p, *Biochemistry 41*, 6438−6448.
23. Dix, D., Bridgham, J., Broderius, M., and Eide, D. (1997) Characterization of the FET4 protein of yeast. Evidence for a direct role in the transport of iron, *J. Biol. Chem. 272*, 11770−11777.
24. Yamaguchi-Iwai, Y., Stearman, R., Dancis, A., and Klausner, R. D. (1996) Iron-regulated DNA binding by the AFT1 protein controls the iron regulon in yeast, *EMBO J. 15*, 3377−3384.
25. Wang, T.-P., Quintanar, L., Severance, S., Solomon, E. I., and Kosman, D. J. (2003) Targeted suppression of the ferroxidase and iron trafficking activities of the multicopper oxidase, Fet3p, from *Saccharomyces cerevisiae*, *J. Biol. Inorg. Chem. 8*, 611−620.
26. Segel, I. (1975) *Enzyme Kinetics*, pp 203−206, Wiley-Interscience, New York.
27. Bonaccorsi di Patti, M. C., Paronetto, M. P., Dolci, V., Felice, M. R., Lania, A., and Musci, G. (2001) Mutational analysis of the iron binding site of *Saccharomyces cerevisiae* ferroxidase Fet3. An in vivo study, *FEBS Lett. 508*, 475−478.
28. Taylor, A. B., Stoj, C. S., Ziegler, L., Kosman, D. J., and Hart, P. J. (2005) The copper−iron connection in biology: structure of the yeast metallo-oxidase, Fet3p, *Proc. Natl. Acad. Sci. U.S.A. 102*, 15459−15464.
29. Quintanar, L., Gebhard, M., Wang, T.-P., Kosman, D. J., and Solomon, E. I. (2004) Ferrous binding to the multicopper oxidases *Saccharomyces cerevisiae* Fet3p and human ceruloplasmin: contributions to ferroxidase activity, *J. Am. Chem. Soc. 126*, 6579−6589.
30. Fersht, A. R. (1999) in *Structure and Mechanism in Protein Science*, pp 350−355, W. H. Freeman, New York.
31. Ackers, G. K., and Smith, F. R. (1985) Effects of site-specific amino acid modification on protein interactions and biological function, *Annu. Rev. Biochem. 54*, 597−629.
32. Jencks, W. P. (1981) On the attribution and additivity of binding energies, *Proc. Natl. Acad. Sci. U.S.A. 78*, 4046−4050.
33. Mildvan, A. S., Weber, D. J., and Kuliopulos, A. (1992) Quantitative interpretation of double mutations of enzymes, *Arch. Biochem. Biophys. 294*, 327−340.
34. Wells, J. A. (1990) Additivity of mutational effects in proteins, *Biochemistry 29*, 8509−8517.
35. Anderson, K. S. (1999) Fundamental mechanisms of substrate channeling, *Methods Enzymol. 308*, 111−145.
36. Spivey, H. O., and Ovadi, J. (1999) Substrate channeling, *Methods 19*, 306−321.
37. Martell, A. E., and Motekaitis, R. J. (1992) *Determination and Use of Stability Constants*, 2nd ed., John Wiley & Sons, New York.
38. Askwith, C., Eide, D., Van Ho, A., Bernard, P. S., Li, L., Davis-Kaplan, S., Sipe, D. M., and Kaplan, J. (1994) The *FET3* gene of *S. cerevisiae* encodes a multicopper oxidase required for ferrous iron uptake, *Cell 76*, 403−410.
39. Miles, E. W., Rhee, S., and Davies, D. R. (1999) The molecular basis of substrate channeling, *J. Biol. Chem. 274*, 12193−12196.
40. Ovadi, J., and Saks, V. (2004) On the origin of intracellular compartmentation and organized metabolic systems, *Mol. Cell. Biochem. 256−257*, 5−12.
41. Rakus, D., Pasek, M., Krotkiewski, H., and Dzugaj, A. (2004) Interaction between muscle aldolase and muscle fructose 1,6-bisphosphatase results in the substrate channeling, *Biochemistry 43*, 14948−14957.
42. Huang, X., Holden, H. M., and Raushel, F. M. (2001) Channeling of substrates and intermediates in enzyme-catalyzed reactions, *Annu. Rev. Biochem. 70*, 149−180.
43. Olsson, U., Billberg, A., Sjovall, S., Al-Karadaghi, S., and Hansson, M. (2002) *In vivo* and *in vitro* studies of *Bacillus subtilis* ferrochelatase mutants suggest substrate channeling in the heme biosynthesis pathway, *J. Bacteriol. 184*, 4018−4024.
44. Seifert, G. J., Barber, C., Wells, B., Dolan, L., and Roberts, K. (2002) Galactose biosynthesis in *Arabidopsis*: genetic evidence for substrate channeling from UDP-D-galactose into cell wall polymers, *Curr. Biol. 12*, 1840−1845.
45. Licata, V. J., and Ackers, G. K. (1995) Long-range, small magnitude nonadditivity of mutational effects in proteins, *Biochemistry 34*, 3133−3139.
46. Huffman, D. L., and O'Halloran, T. V. (2001) Function, structure, and mechanism of intracellular copper trafficking proteins, *Annu. Rev. Biochem. 70*, 677−701.
47. Xiao, Z., Loughlin, F., George, G. N., Howlett, G. J., and Wedd, A. G. (2004) C-terminal domain of the membrane copper transporter Ctr1 from *Saccharomyces cerevisiae* binds four Cu(I) ions as a cuprous-thiolate polynuclear cluster: sub-femtomolar Cu(I) affinity of three proteins involved in copper trafficking, *J. Am. Chem. Soc. 126*, 3081−3090.
48. Xiao, Z., and Wedd, A. G. (2002) A C-terminal domain of the membrane copper pump Ctr1 exchanges copper(I) with the copper chaperone Atx1, *Chem. Commun.*, 588−589.
49. Huffman, D. L., and O'Halloran, T. V. (2000) Energetics of copper trafficking between the Atx1 metallochaperone and the intracellular copper transporter, Ccc2, *J. Biol. Chem. 275*, 18611−18614.
50. Rae, T. D., Schmidt, P. J., Pufahl, R. A., Culotta, V. C., and O'Halloran, T. V. (1999) Undetectable intracellular free copper: the requirement of a copper chaperone for superoxide dismutase, *Science 284*, 805−808.
51. Milani, M., Pesce, A., Bolognesi, M., Bocedi, A., and Ascenzi, P. (2003) Substrate channeling: molecular bases, *Biochem. Mol. Biol. Educ. 31*, 228−233.
52. Maynard, E. L., and Lindahl, P. A. (2001) Catalytic coupling of the active sites in acetyl-CoA synthase, a bifunctional CO-channeling enzyme, *Biochemistry 40*, 13262−13267.
53. Dobbek, H., Svetlitchnyi, V. Gremer, L., Huber, R. and Neyer, Ol. (2001) Crystal structure of a corbon monoxide dehydrogenase reveals a [Ni4Fe-5S] cluster, *Science 293*, 1281−1285.
54. Treffry, A., Bauminger, E. R., Hechel, D., Hodson, N. W., Nowik, I., Yewdall, S. J., and Harrison, P. M. (1993) Defining the roles of the threefold channels in iron uptake, iron oxidation and iron-core formation in ferritin: a study aided by site-directed mutagenesis, *Biochem. J. 296*, 721−728.
55. Santambrogio, P., Levi, S., Cozzi, A., Corsi, B., and Arosio, P. (1996) Evidence that the specificity of iron incorporation into homopolymers of human ferritin L- and H-chains is conferred by the nucleation and ferroxidase centres, *Biochem. J. 314*, 139−144.
56. Liu, X., and Theil, E. C. (2004) Ferritin reactions: direct identification of the site for the diferric peroxide reaction intermediate, *Proc. Natl. Acad. Sci. U.S.A. 101*, 8557−8562.

BI052173C